THE JOURNAL OF BIOLOGICAL CHEMISTRY VOL. 281, NO. 8, pp. 4983–4992, February 24, 2006

A Comparative Study of Uracil-DNA Glycosylases from Human and Herpes Simplex Virus Type 1*

Received for publication, August 18, 2005, and in revised form, November 18, 2005 Published, JBC Papers in Press, November 22, 2005, DOI 10.1074/jbc.M509137200

Kuakarun Krusong[‡1], **Elisabeth P. Carpenter**[§], **Stuart R. W. Bellamy**[¶], **Renos Savva**[‖], **and Geoff S. Baldwin**[‡2]

From the [‡]*Division of Molecular Biosciences and the* [§]*Centre for Structural Biology, Imperial College London, South Kensington, London SW7 2AZ, United Kingdom, the* [¶]*Department of Biochemistry, University of Bristol, University Walk, Bristol BS8 1TD, United Kingdom, and the* [‖]*School of Crystallography, Birkbeck College, Malet Street, London WC1E 7HX, United Kingdom*

Uracil-DNA glycosylase (UNG) is the key enzyme responsible for initiation of base excision repair. We have used both kinetic and binding assays for comparative analysis of UNG enzymes from humans and herpes simplex virus type 1 (HSV-1). Steady-state fluorescence assays showed that hUNG has a much higher specificity constant (k_{cat}/K_m) compared with the viral enzyme due to a lower K_m. The binding of UNG to DNA was also studied using a catalytically inactive mutant of UNG and non-cleavable substrate analogs (2′-deoxypseudouridine and 2′-α-fluoro-2′-deoxyuridine). Equilibrium DNA binding revealed that both human and HSV-1 UNG enzymes bind to abasic DNA and both substrate analogs more weakly than to uracil-containing DNA. Structure determination of HSV-1 D88N/H210N UNG in complex with uracil revealed detailed information on substrate binding. Together, these results suggest that a significant proportion of the binding energy is provided by specific interactions with the target uracil. The kinetic parameters for human UNG indicate that it is likely to have activity against both U·A and U·G mismatches *in vivo*. Weak binding to abasic DNA also suggests that UNG activity is unlikely to be coupled to the subsequent common steps of base excision repair.

Uracil-DNA glycosylase (UNG)[3] is the primary enzyme responsible for the removal of uracil from DNA. Uracil can arise in DNA either by the misincorporation of dUTP during DNA synthesis, which results in a U·A base pair, or by the spontaneous deamination of cytosine. Approximately 100 cytosine deamination events cell^{-1} day^{-1} are expected in human cells (1), producing a promutagenic U·G mismatch in DNA. If unrepaired, this will lead to an A·T transition mutation following DNA replication.

UNG is one of the initiating DNA glycosylases of the base excision repair pathway and is responsible for the specific recognition and removal of uracil. It removes uracil by cleavage of the *N*-glycosidic bond between the uracil and the deoxyribose backbone, leaving an apyrimidinic (AP) site (2). AP sites are themselves highly mutagenic and are further repaired by the common downstream enzymes of the base excision repair pathway (3). The first common repair step is an AP endonuclease, which cleaves the DNA backbone at the abasic site (4).

UNG enzymes have been identified in a wide variety of organisms, including human, *Escherichia coli*, and herpes simplex virus type 1 (HSV-1). They are well conserved; the HSV-1 and human enzymes have 39% sequence identity, whereas the HSV-1 and *E. coli* enzymes are 49% identical. They are also highly conserved at the structural level (5–7). The structure of human (h) UNG in complex with DNA has revealed that it binds uracil by flipping the target nucleotide out of the double helix and into the active-site pocket (6, 8). The DNA-binding pocket of UNG is highly specific for uracil in DNA. Other DNA bases and uracils in RNA are excluded from this DNA-binding pocket due to unfavorable steric and hydrogen bond interactions (5, 6).

A number of previous studies on both the human and HSV-1 UNG enzymes have indicated possible differences in their catalytic behavior. Notably, hUNG has been reported to bind tightly to its abasic product DNA, and it has been proposed that the action of hUNG is coupled to the common base excision repair steps via AP endonuclease (9). In comparison, HSV-1 UNG has been observed to bind product DNA only weakly (10, 11), making coupling of these two events unlikely in the viral enzyme. Furthermore, hUNG has been cited as having a higher K_m value (8, 12, 13) than we observed for HSV-1 UNG (10), and this has informed the description of hUNG as having a single function in post-replicative repair of U·A mismatches (14).

In light of these reported differences between the viral and human UNG enzymes, we decided to investigate both enzymes in kinetic and DNA binding studies. The objective was to precisely identify any differences between these two highly related DNA repair enzymes, with a view to further defining their functional roles as well as exploring the potential of viral UNG as a therapeutic target. A previous report has indicated that nucleotide analogs may provide specific inhibitors for the HSV-1 enzyme (15). We therefore wished to investigate the DNA binding of both human and HSV-1 UNG enzymes to non-cleavable substrate analogs both as a probe to investigate protein-DNA interactions and to further explore the possibility of finding specific inhibitors of viral UNG.

We investigated the catalytic rates and DNA binding properties of both wild-type and mutant forms of human and viral UNG using both biochemical and biophysical assays. These included quench reactions to monitor the rate of *N*-glycosyl hydrolysis and a fluorescence assay to follow steady-state reactions. Furthermore, the binding of the human and HSV-1 UNG enzymes to substrate DNA and abasic product DNA was examined by fluorescence anisotropy. Catalytically inactive mutant enzymes were used in studies of the binding of UNG to uracil-containing substrates. In addition, the binding activity of wild-type UNG was measured using the non-hydrolyzable substrate analogs 2′-deoxypseudouridine (dΨrd) and 2′-α-fluoro-2′-deoxyuridine (α-FdUrd). We also performed crystallographic analysis of HSV-1 mutant UNG to

* This work was supported in part by the Biotechnology and Biological Sciences Research Council. The costs of publication of this article were defrayed in part by the payment of page charges. This article must therefore be hereby marked "*advertisement*" in accordance with 18 U.S.C. Section 1734 solely to indicate this fact.

The atomic coordinates and structure factors (codes 2C56 and 2C53) have been deposited in the Protein Data Bank, Research Collaboratory for Structural Bioinformatics, Rutgers University, New Brunswick, NJ (http://www.rcsb.org/).

[1] Supported by a studentship from the Royal Thai Government.

[2] To whom correspondence should be addressed: Div. of Molecular Biosciences, Imperial College London, Sir Alexander Fleming Bldg., South Kensington, London SW7 2AZ, UK. Tel.: 44-20-7594-5228; Fax: 44-20-7584-2056; E-mail: g.baldwin@imperial.ac.uk.

[3] The abbreviations used are: UNG, uracil-DNA glycosylase; AP, apyrimidinic; HSV-1, herpes simplex virus type 1; h, human; dΨrd, 2′-deoxypseudouridine; α-FdUrd, 2′-α-fluoro-2′-deoxyuridine; 2-AP, 2-aminopurine.

compare the active-site structure and mode of uracil binding to the wild-type enzyme.

MATERIALS AND METHODS

Plasmid Constructions—HSV-1 wild-type UNG was prepared using the recombinant plasmid pTS106.1 (5). Site-directed mutagenesis was carried out on pTS106.1 to construct the HSV-1 D88N and H210N UNG single mutants. The HSV-1 D88N/H210N UNG double mutant was constructed by cloning an XbaI fragment of the pH210N plasmid, which contains the H210N mutation, into the pD88N plasmid. All mutants were verified by sequencing.

The recombinant hUNG plasmid pUNG15 was purchased from American Type Culture Collection. The truncated h*UNG* gene encoding amino acids 84–304 of hUNG was subcloned into expression vector pRSET-B (Invitrogen) using NcoI/HindIII restriction sites. The DNA fragment encoding the enterokinase recognition site located between the N-terminal polyhistidine tag and the truncated h*UNG* gene was deleted by NcoI/NheI digestion, fill-in reaction (16), and plasmid religation, resulting in pHUNG4. The D145N and H268N mutations were introduced into pHUNG4 by site-directed mutagenesis. Human D145N/H268N UNG was subsequently generated by site-directed mutagenesis using the plasmid containing the D145N h*UNG* gene as a template. All mutants were verified by sequencing.

Protein Overexpression and Purification—HSV-1 UNG was overexpressed and purified as described previously (10). The D88N, H210N, and D88N/H210N mutant enzymes were expressed and purified from a construct in exactly the same manner. hUNG and its mutant enzymes were expressed in *E. coli* BH156. The cultures were grown in LB broth at 37 °C to $A_{600} = 0.8$ before induction with 1 mM isopropyl 1-thio-β-D-galactopyranoside. The cultures were grown for an additional 3 h at 37 °C before the cells were harvested. The harvested cells were lysed by sonication in buffer containing 20 mM Tris (pH 7.6), 50 mM imidazole, 300 mM NaCl, and a tablet of EDTA-free protease inhibitors (Roche Applied Science). The lysate was clarified by centrifugation at 40,000 rpm for 45 min. The clarified lysate was loaded onto a nickel-Sepharose column equilibrated in 20 mM Tris (pH 7.6), 50 mM imidazole, and 300 mM NaCl. After washing, the UNG enzyme was eluted from the column with a gradient of 50–500 mM imidazole. The fractions were assayed by SDS-PAGE, and those containing UNG were pooled and concentrated by ultrafiltration. The concentrated fractions were diluted with 20 mM Tris (pH 7.6), 1 mM EDTA, and 10% glycerol so that the NaCl concentration was <0.02 M. The partially purified protein was then applied to a poly(U)-Sepharose affinity column equilibrated in 20 mM Tris (pH 7.6), 1 mM EDTA, and 10% glycerol; and after washing, the UNG enzyme was eluted with a gradient of 0–1 M NaCl. The pure enzyme was then concentrated by ultrafiltration. The concentration of the protein was calculated from the absorbance at 280 nm based on an extinction coefficient of 48.9×10^3 M^{-1} cm^{-1}.

DNA Synthesis and Purification—Oligodeoxynucleotides were synthesized by MWG Biotech. All modifications were incorporated into oligonucleotides at the point of synthesis using conventional phosphoramidite chemistry. The phosphoramidites of 2′-dUrd, dΨrd, α-FdUrd, 2-aminopurine (2-AP), and hexachlorofluorescein were also supplied by MWG Biotech. Oligonucleotides were purified by high pressure liquid chromatography as described previously (17). Double-stranded substrates and abasic oligonucleotides were made as described previously (10).

Kinetic Assays—Steady-state fluorescence spectra were measured on a HORIBA Jobin Yvon FluoroMax 3 spectrofluorometer. The 2-AP fluorescence was recorded with an excitation wavelength of 310 nm and an emission wavelength of 370 nm using a 5-mm cuvette. Steady-state fluorescence assays were performed at 25 °C in 50 mM Tris-HCl (pH 7.6), 1 mM EDTA, 50 mM NaCl, 0.1 mg ml^{-1} bovine serum albumin, and 2 mM $MgCl_2$ using the hUNG enzyme to give a final concentration of 0.5, 1.0, or 2.0 nM. The endpoint of the reaction was determined by addition of the second aliquot of high concentration UNG. The initial velocity (μM s^{-1}) was then calculated from the initial linear progression in fluorescence and the total change in fluorescence. The rate (s^{-1}) was calculated by dividing the initial velocity by the total enzyme concentration.

Single turnover quench reactions were performed at 25 °C with ^{32}P-labeled Urd substrate (0.1 μM; see Table 1) and mutant UNG enzymes (1 μM) in standard reaction buffers (HSV-1 UNG: 50 mM Tris-HCl (pH 8.0), 1 mM EDTA, 150 mM NaCl, and 0.1 mg ml^{-1} bovine serum albumin; and hUNG: 50 mM Tris-HCl (pH 7.6), 1 mM EDTA, 50 mM NaCl, and 0.1 mg ml^{-1} bovine serum albumin). The assay was otherwise performed as described previously (18).

Competitive DNA Binding Assays—Competitive equilibrium DNA binding assays were performed by fluorescence anisotropy using the FluoroMax 3 spectrofluorometer fitted with automated polarization filters. Data were recorded using an excitation wavelength of 530 nm and an emission wavelength of 555 nm. The binding assays were conducted at 25 °C in reaction buffer by titrating increasing concentrations of the unlabeled ssU oligonucleotide into a fixed concentration of the fluorescent HU oligonucleotide and D88N/H210N UNG. Data were analyzed following the method of Reid *et al.* (19) using the program Scientist (MicroMath Research).

Equilibrium DNA Binding Assays—Equilibrium DNA binding assays were performed by fluorescence anisotropy using the same spectroscopic settings described above to examine the binding of the wild-type and mutant UNG enzymes to the 5′-hexachlorofluorescein-labeled oligonucleotides (Table 1). The binding assays were conducted at 25 °C in reaction buffer by titrating fixed concentrations of the fluorescent DNA with increasing amounts of the enzyme. The observed anisotropy was plotted against the concentration of enzyme, and the data were fitted to the quadratic binding equation (Equation 1) using GraFit Version 5.0,

$$A = A_D + (A_{DE} - A_D) \times (((K_d + [E]_0 + [DNA]_T) - \sqrt{(-K_d - [E]_0 - [DNA]_T^2 - 4[E]_0[DNA]_T)})/(2[DNA]_T)) \quad \text{(Eq. 1)}$$

where $[DNA]_T$ is the concentration of DNA used in each experiment, A is the observed anisotropy, A_D is the anisotropy for free DNA, A_{DE} is the anisotropy for enzyme-bound DNA, K_d is the equilibrium dissociation constant, and $[E]_0$ is the total enzyme concentration.

Crystallization, Data Collection, and Structure Determination and Refinement—Crystals of HSV-1 D88N/H210N UNG were obtained in microbatch experiments at 25 °C at 30 mg ml^{-1} protein in 6% polyethylene glycol 4000 and 40 mM imidazole (pH 6.8). The D88N/H210N UNG-uracil complexes were obtained by soaking native crystals in 11% polyethylene glycol 4000, 42 mM imidazole (pH 6.8), and 20 mM 2′-dUrd (Sigma) for 16 h.

Diffraction data were collected on a Quantum 4 CCD detector (Area Detection Systems Corp.) with 0.978-Å radiation on beamline 9.6 of the Daresbury Synchrotron Radiation Source (Cheshire, UK). Diffraction images were processed using Denzo and Scalepack (HKL Research, Inc). Parameters for the data collection and processing are given in Table 2. The structure of HSV-1 D88N/H210N UNG was determined by molecular replacement using molrep (20) and the structure of HSV-1 wild-type UNG (Protein Data Bank code 1UDG) as a search model. The best molecular replacement solution gave a correlation coefficient of 0.470

and an *R*-factor of 0.438, with corresponding values for the next highest peak of 0.252 and 0.528. The protein model transformed by the molecular replacement solution was refined against the observed diffraction data using CNS (21). The $F_o - F_c$ maps reveal electron density features consistent with the Asn^{210} and Asn^{88} mutations.

Subsequent cycles of manual model building were performed using the program O (22). The structure of D88N/H210N UNG was further refined by stereochemically restrained simulated annealing and positional refinement with the program CNS (21). Ordered solvent molecules were placed into $F_o - F_c$ maps using the program ARP/wARP (23). Progress was monitored throughout by the consistent decrease in the crystallographic *R*-factor and verified by cross-validation by a corresponding decrease in R_{free}. The quality of the refined model was determined using the programs PROCHECK (24) and WHATCHECK (25). The refinement statistics of D88N/H210N UNG are shown in Table 2.

TABLE 1

Substrates used in kinetic and equilibrium binding assays

The chromophore hexachlorofluorescein (HEX) was incorporated at the 5′-end during synthesis. The double-stranded substrates (HU·G and HAP:G) were made by annealing the appropriate strands.

Oligonucleotide	Sequence
Steady-state fluorescence[a]	
1U	5′-GAC TAP UAA TGA CTG CG-3′
1U·G	5′-GAC TA**P** **U**AA TGA CTG CG-3′
	3′-CTG ATT GTT ACT GAC GC-5′
1U·A	5′-GAC TA**P** **U**AA TGA CTG CG-3′
	3′-CTG ATT ATT ACT GAC GC-5′
Single turnover assays[b]	
ssU	5′-GAC TAA UAA TGA CTG CG-3′
Binding assays	
HU (U = 2′-dUrd)	5′-(HEX) GAC TAA **U**AA TGA CTG CG-3′
HU·G (U = 2′-dUrd)	5′-(HEX) GAC TAT **U**AA TGA CTG CG-3′
	3′-CTG ATA GTT ACT GAC GC-5′
HAP (*X* = abasic)	5′-(HEX) GAC TAA *X*AA TGA CTG CG-3′
HAP·G (*X* = abasic)	5′-(HEX) GAC TAT *X*AA TGA CTG CG-3′
	3′-CTG ATA GTT ACT GAC GC-5′
dΨrd (*X* = dΨrd)	5′-(HEX) GAC TAA *X*AA TGA CTG CG-3′
α-FdUrd (*X* = α-FdUrd)	5′-(HEX) GAC TAA *X*AA TGA CTG CG-3′

[a] Oligonucleotides for steady-state fluorescence assays were synthesized with 2-AP (P) incorporated next to the uracil base (1U). The double-stranded substrates (1U·G and 1U·A) were made by annealing the appropriate strands.
[b] The oligonucleotide for single turnover assays was 5′-labeled with ^{32}P.

Data for HSV-1 D88N/H210N UNG in complex with uracil were collected on the Quantum 4 CCD detector with 0.87-Å radiation on beamline 9.6 of the Daresbury Synchrotron Radiation Source. The complex crystal had the same space group as the native crystal. Data collection statistics are shown in Table 2. The structure of D88N/H210N UNG in complex with uracil was determined by molecular replacement using molrep (20) and the structure of native D88N/H210N UNG as a search model. The correct solution gave the highest correlation coefficient of 0.507 and an *R*-factor of 0.400, with corresponding values for the next solution of 0.336 and 0.501, respectively. The model of the complex was refined and rebuilt as described above. The $F_o - F_c$ maps indicate the presence of a uracil base in the active site of UNG. The uracil was constructed and refined with the protein model using CNS (21). The final model gave refinement statistics as shown in Table 2.

RESULTS

Steady-state Analysis—Steady-state reactions were performed with hUNG to determine its kinetic parameters under the same conditions that had been previously used for HSV-1 UNG (10). The fluorescent base analog 2-AP was used to monitor the kinetics of glycosidic bond cleavage by incorporation next to a uracil base in oligonucleotide substrates (Table 1). Because the quantum yield of 2-AP is very sensitive to its environment and displays strong quenching when stacked in DNA (26), removal of the uracil base adjacent to 2-AP by UNG results in a large increase in fluorescence (27). We have previously demonstrated that incorporation of 2-AP does not affect the binding of the UNG enzyme to the oligonucleotide (10).

hUNG reactions were performed with a single-stranded oligonucleotide substrate (1U) and double-stranded forms of the substrate containing either a U·G mismatch or a U·A base pair (1U·G and 1U·A, respectively). The rate constants showed a hyperbolic dependence upon the substrate concentration, and the data were fitted to the Michaelis-Menten equation (Fig. 1), giving the steady-state parameters k_{cat} and K_m. We also determined that removal of the N-terminal His tag from hUNG had no impact on the catalytic constants (data not shown). The kinetic parameters for hUNG with different substrates are shown compared with those for HSV-1 UNG (Table 3) (10). The kinetic data show an 8–50-fold higher k_{cat}/K_m value for hUNG compared with that for

TABLE 2

Crystallographic statistics

The Protein Data Bank accession codes are 2C56 for HSV-1 D88N/H210N UNG and 2C53 for HSV-1 D88N/H210N UNG with dUrd. r.m.s.d., root mean square deviation.

	Crystals	
	D88N/H210N UNG	**D88N/H210N UNG-uracil complex**
Data collection		
Resolution (Å)	30.0 to 2.1	15.0 to 1.8
Space group	$P2_1$	$P2_1$
Unit cell dimensions	$a = 42.04$, $b = 61.117$, $c = 43.392$, $\alpha = 90$, $\beta = 92.251$, $\gamma = 90$	$a = 42.406$, $b = 61.161$, $c = 43.620$, $\alpha = 90$, $\beta = 93.15$, $\gamma = 90$
Measured reflections	47,672	63,757
Unique reflections	12,927	19,411
Overall completeness	99.9	93.7
High resolution shell	100 (2.18 to 2.10)	63.1 (1.86 to 1.80)
Overall R_{merge}	8.5	7.5
High resolution shell	22.0	25.8
Overall I/σ	12.5	13.8
Highest resolution shell I/σ	5.3	2.3
Structure refinement		
No. of working reflections	12,266	18,435
No. of free reflections	646	961
R-factor (%)	0.1507	0.1641
R_{free} (%)	0.2118	0.2157
Average *B*-factor	14.235	16.177
No. of atoms	2102	2112
r.m.s.d. bond distances (Å)	0.016	0.017
r.m.s.d. bond angles	1.699°	1.683°

HSV-1 UNG. This represents a significantly increased catalytic efficiency for hUNG.

Active-site Mutations—The active site of UNG contains catalytic Asp and His residues that are highly conserved throughout all UNG enzymes and that have been demonstrated to be involved in catalysis (5, 6, 28). We have made Asn mutations for both of these residues, both singly and in combination for the human and HSV-1 UNG enzymes, for the purpose of generating inactive mutant enzymes for DNA binding studies. Furthermore, we intend to explore the role of these residues in catalysis and substrate binding.

The activity of the UNG mutants was monitored under single turnover conditions using the quench assay with the ^{32}P-labeled ssU oligonucleotide (18). Under these conditions, the substrate is in excess over the enzyme; and hence, only a single turnover of the reaction occurs: under saturating conditions, the accumulation of product corresponds directly to the rate of *N*-glycosidic bond cleavage. The observed rate of cleavage (k_{obs}) was determined by fitting the accumulation of product to either a single exponential or a linear equation.

Reactions were performed under saturating conditions with a 10-fold excess of the single mutant UNG enzymes (human D145N and H268N and HSV-1 D88N and H210N) over the ^{32}P-labeled substrate. The reactions demonstrated that the single mutants of UNG contain some residual activity (Fig. 2). However, the human D145N/H268N and HSV-1 D88N/H210N UNG double mutants showed no UNG activity even after 24 h with a 10-fold excess of the enzyme (data not shown).

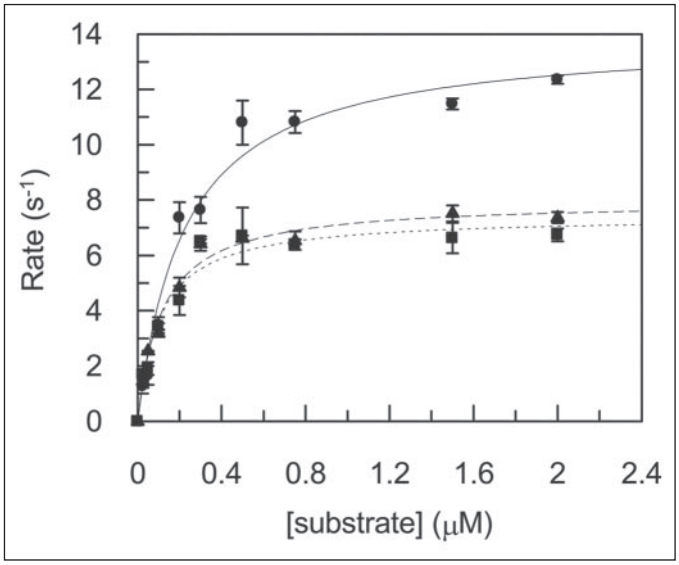

FIGURE 1. **Steady-state analysis of hUNG.** Steady-state reactions were performed by monitoring the fluorescence of 2-AP-containing substrates (see "Materials and Methods") after addition of hUNG. Rates were determined from the initial increase in fluorescence at different concentrations of substrates and normalized for enzyme concentration. The observed rates are shown plotted against concentration for the substrates 1U (●), U·G (▲), and U·A (■). The data are shown with the best fit to the Michaelis-Menten equation with the following values: 1U(——), $k_{cat} = 13.9 \pm 0.7\ s^{-1}$ and $K_m = 0.22 \pm 0.04\ \mu M$; 1U·G (– – –), $k_{cat} = 8.0 \pm 0.3\ s^{-1}$ and $K_m = 0.12 \pm 0.02\ \mu M$; and 1U·A (····), $k_{cat} = 7.4 \pm 0.4\ s^{-1}$ and $K_m = 0.1 \pm 0.02\ \mu M$.

Equilibrium DNA Binding—To prevent turnover of substrate in DNA binding experiments, it is necessary to use either inactive enzyme mutants or substrates that are refractory to cleavage. In this study, we used both approaches. As described above, the human D145N/H268N and HSV-1 D88N/H210N UNG double mutants had no activity even after 24 h under standard reaction conditions and are thus suitable for use in DNA binding studies. In addition, the human H268N and HSV-1 H210N UNG enzymes were deemed sufficiently inactive to be used in binding assays with uracil-containing substrates. However, the human D145N and HSV-1 D88N UNG single mutants had sufficient residual activity that they could be used only with the non-cleavable substrate analogs and abasic product DNA.

We used two non-cleavable substrate analogs (dΨrd and α-FdUrd). The pucker of the ribose sugar is largely determined by the electronegativity of the 2′-substituent; hence, RNA has a C-3′-*endo* sugar pucker, whereas DNA has a C-2′-*endo* sugar pucker (29). Similarly, both the α- and β-2′-fluorouridine derivatives favor the C-3′-*endo* pucker (30–32). The β-isomer has been suggested to be the better uridine analog (33); in 2-AP fluorescence binding assays with *E. coli* UNG, it gave a stronger signal; although the α-isomer was also observed to be bound by this enzyme, a K_d was not reported for this isomer. The β-isomer has also been reported to be a specific inhibitor of HSV-1 UNG (15). In this study, we used the commercially available α-isomer.

The binding of DNA by UNG has been observed using 5′-hexachlorofluorescein-labeled DNA substrates. When proteins bind the fluorescently labeled DNA, it leads to a change in the rotational diffusion of the fluorophore due to the change in the molecular mass of the protein-DNA complex relative to free DNA. This in turn results in an increase in fluorescence anisotropy and has been shown to be an ideal method for monitoring the binding of DNA by proteins in solution (34). The advantage of this technique is that the DNA is free to move in solution. Moreover, the fluorescence reporter group is far removed from the target uracil and thus provides a measure of DNA binding that is independent of other conformational transitions associated with damage recognition.

It is of course important to determine that the hexachlorofluorescein reporter group does not interfere with DNA binding by UNG. We have therefore examined this by performing a competition binding experiment. Sufficient HSV-1 D88N/H210N UNG was mixed with the labeled HU oligonucleotide to form an enzyme-DNA complex, and the labeled DNA was then competed away with the unlabeled ssU oligonucleotide. This resulted in a decrease in the observed anisotropy, which could be fitted to a competitive binding model following the method described by Reid *et al.* (19). This gave a K_d of 4.9 nM for the unlabeled ssU oligonucleotide (Fig. 3), compared with a K_d of 10 nM for the hexachlorofluorescein-labeled HU oligonucleotide (Table 4; see below). This demonstrates that the hexachlorofluorescein reporter group does not interfere with DNA binding by UNG for the substrates used in this study.

TABLE 3

Comparison of steady-state data of the human and HSV-1 UNG enzymes

Steady-state reactions were performed with the substrates shown in Table 1 using fluorescence assays. The kinetic parameters were obtained by fitting data to the Michaelis-Menten equation. The parameters k_{cat} and K_m for HSV-1 UNG are from Bellamy and Baldwin (10).

Substrate	hUNG			HSV-1 UNG		
	k_{cat}	K_m	k_{cat}/K_m	k_{cat}	K_m	k_{cat}/K_m
	s^{-1}	μM	$\mu M\ s^{-1}$	s^{-1}	μM	$\mu M\ s^{-1}$
1U	13.9 ± 0.7	0.22 ± 0.04	63 ± 15	6.7 ± 0.3	0.9 ± 0.1	7.1 ± 1.1
1U·G	8.0 ± 0.3	0.1 ± 0.02	74 ± 19	2.4 ± 0.2	0.9 ± 0.2	2.7 ± 0.8
1U·A	7.4 ± 0.4	0.12 ± 0.02	67 ± 14	2.1 ± 0.1	1.6 ± 0.2	1.3 ± 0.2

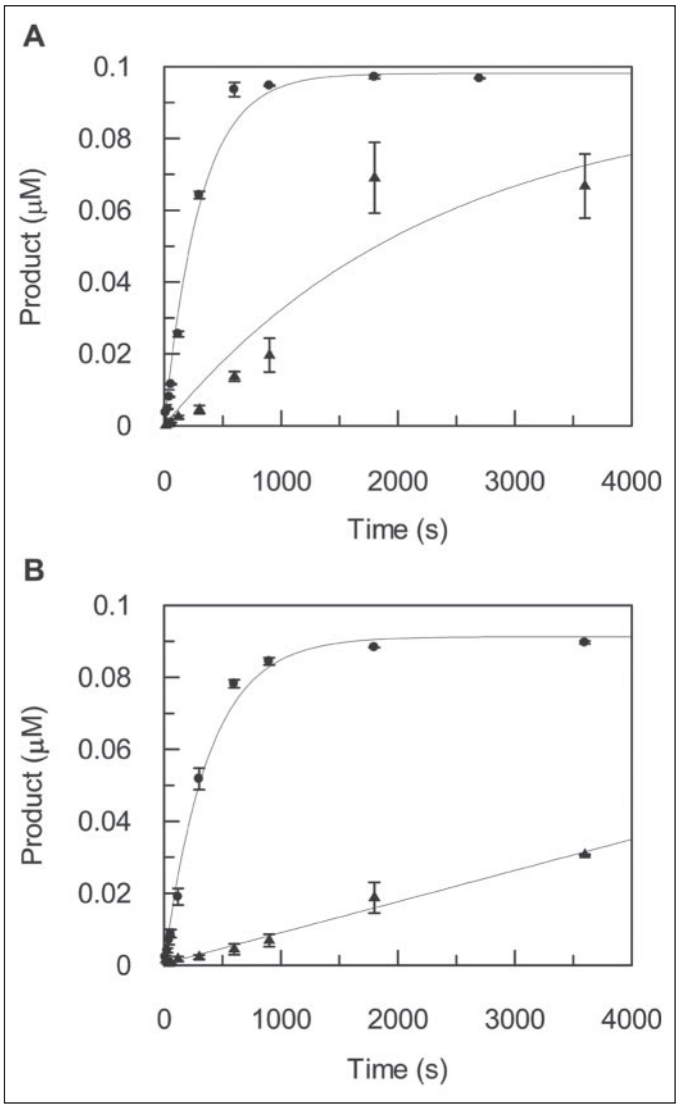

FIGURE 2. **Single turnover analysis of single mutant UNG enzymes.** Quench reactions were performed with a 10-fold excess of the mutant enzymes over the ^{32}P-labeled ssU substrate (1 μM mutant UNG to 0.1 μM ssU substrate), with the other conditions as described under "Materials and Methods." *A*, data for the human D145N (●) and H268N (▲) UNG single mutants are shown with the best fit to a single exponential equation with the following values: human D145N UNG, $k_{obs} = 3.3 \times 10^{-3} \pm 4 \times 10^{-4}$ s^{-1}; and human H268N UNG, $k_{obs} = (4.0 \pm 2) \times 10^{-4}$ s^{-1}. *B*, data for HSV-1 D88N UNG (●) are shown with the best fit to a single exponential equation with $k_{obs} = 2.7 \times 10^{-3} \pm 4 \times 10^{-4}$ s^{-1}. Data for HSV-1 H210N UNG are shown (▲) with the best fit to a linear equation. An estimated k_{obs} for HSV-1 H210N UNG was calculated from the linear gradient (μM^{-1} s^{-1}) and normalized to the total enzyme concentration with $k_{obs} = 8.6 \times 10^{-5} \pm 4 \times 10^{-6}$ s^{-1}.

Direct binding isotherms were obtained by titrating increasing concentrations of enzyme into a fixed concentration of different fluorescent substrates (Table 1). The dissociation constant (K_d) was then determined by plotting the resulting change in anisotropy *versus* enzyme concentration and fitting the data to the quadratic binding equation (Equation 1 under "Materials and Methods"). It should be noted that this equation is free from errors that can arise when the total enzyme concentration is not equal to the free enzyme concentration and so can be used under tight binding conditions.

The inactive human D145N/H268N UNG enzyme produced a tight binding curve with both the single- and double-stranded uracil-containing substrates (HU and HU·G) (Fig. 4*A*). When the wild-type enzyme was examined with the abasic DNAs, the binding was found to be 2 orders of magnitude weaker (Fig. 4*B*). Similar results were also found with the human H268N UNG single mutant (Table 4).

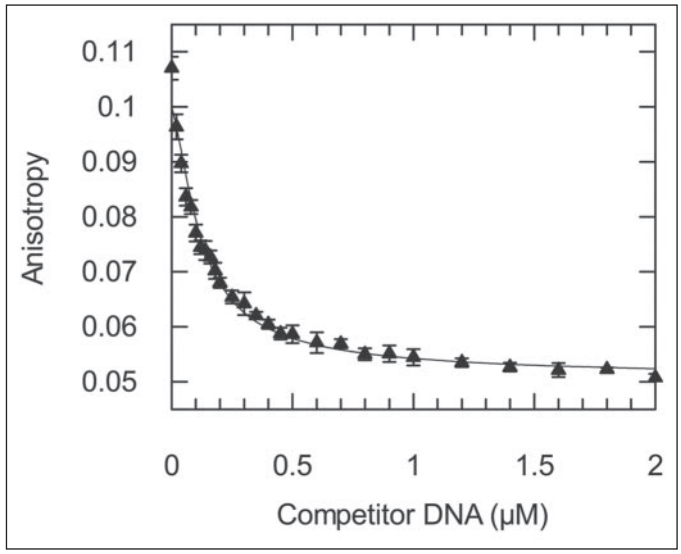

FIGURE 3. **Competitive DNA binding.** A competitive binding experiment was performed by mixing HSV-1 D88N/H210N UNG (0.12 μM) with the HU oligonucleotide (0.1 μM). The fluorescence anisotropy was then measured as the unlabeled ssU oligonucleotide was titrated in up to 2.0 μM. The data are shown with the best fit to the competitive binding model (see "Materials and Methods") with the following values: total DNA concentration = 0.1 μM; total enzyme concentration = 0.12 μM; anisotropy of free DNA = 0.051; anisotropy of bound DNA = 0.113; K_d for labeled HU DNA = 0.01 μM (Table 4); and K_{d1} for unlabeled ssU competitor DNA = 0.0049 μM.

Binding of Substrate Analogs—DNA binding was also investigated with the wild-type and mutant hUNG enzymes and the non-cleavable substrate analogs Ψrd and α-FdUrd. The wild-type enzyme bound both Ψrd and α-FdUrd DNAs ~2 orders of magnitude more weakly compared with the mutant enzymes with uracil-containing DNA (Fig. 5*A*). We therefore considered that this discrepancy could be due to two causes: the mutant UNG enzymes might bind uracil-containing DNA anomalously tightly; alternatively, the mutants may bind DNA in a very similar manner to the wild-type enzyme, but the non-cleavable analogs that we tested are not good substrate mimics. Intriguingly, a strain hypothesis has been previously proposed for UNG (35), and it is possible that the wild-type enzyme might bind its substrate more weakly compared with a mutant that is unable to exert any strain on the substrate.

This hypothesis was therefore tested by examining the binding of the mutant hUNG enzymes with the non-cleavable substrate analogs Ψrd and α-FdUrd. The human D145N/H268N UNG double mutant bound both substrate analogs with a weak affinity similar to that observed with the wild-type enzyme (Fig. 5*B*). Experiments were also performed with the human D145N and H268N UNG single mutants. In both cases, similar weak binding affinities were also observed (Table 4). This therefore indicates that the inability of UNG to bind Ψrd and α-FdUrd tightly is not due to substrate strain because the mutants, which bound the uracil-containing DNA substrates tightly, bound the DNA analogs weakly. The mutants thus appear to be unable to bind the bases of Ψrd and α-FdUrd in the same manner in which they bind the uracil base in the HU and HU·G oligonucleotides. Indeed, it is striking that the binding affinities of the analog DNAs closely resemble those observed with the abasic product DNA, and it is possible that the DNA binding with Ψrd and α-FdUrd is due to nonspecific interactions with the DNA backbone.

We also extended our previous work on DNA binding by HSV-1 UNG to include the substrate analogs and thus further explore this issue as well as the relatedness of the human and HSV-1 UNG enzymes. The equivalent active-site mutations were investigated with the substrate analog DNAs Ψrd and α-FdUrd. In all cases, HSV-1 UNG exhibited

TABLE 4

Equilibrium binding

The dissociation constants (K_d) for the human and HSV-1 UNG enzymes were determined with a series of substrates (Table 1) by fluorescence anisotropy. These included uracil in both single- and double-stranded DNAs (HU and HU·G), the abasic forms of the HU and HU·G substrates (HAP and HAP:G), and the non-cleavable substrate analogs dΨUrd and α -FdUrd.

	K_d					
	HU	HAP	HU·G	HAP·G	dΨUrd	α-FdUrd
			μM			
hUNG						
H268N	$(0.010 \pm 4) \times 10^{-4}$	4.3 ± 0.3	$(0.033 \pm 9) \times 10^{-3}$	2.9 ± 0.2	2.0 ± 0.3	1.1 ± 0.1
D145N		1.7 ± 0.7		2.9 ± 0.3	2.6 ± 0.8	2.9 ± 0.7
D145N/H268N	$(0.016 \pm 2) \times 10^{-3}$	3.5 ± 0.3	$(0.130 \pm 8) \times 10^{-3}$	4.5 ± 0.3	3.2 ± 0.2	2.2 ± 0.2
Wild-type		6.9 ± 0.7		9.0 ± 0.8	4.4 ± 0.5	6.3 ± 0.6
HSV-1 UNG						
H210N	$(0.005 \pm 7) \times 10^{-4}$	3.9 ± 0.3	$(0.055 \pm 5) \times 10^{-3}$	3.3 ± 0.3	6.1 ± 0.9	1.2 ± 0.2
D88N		4.0 ± 0.3		3.5 ± 0.2	2.0 ± 0.1	1.9 ± 0.1
D88N/H210N	$(0.008 \pm 2) \times 10^{-3}$	5.6 ± 0.6	$(0.068 \pm 7) \times 10^{-3}$	5.3 ± 0.6	4.3 ± 0.2	3.3 ± 0.04
Wild-type		7.2 ± 0.7		8.1 ± 1.6	8.5 ± 0.5	9.4 ± 0.5

exactly the same behavior as its human counterpart (Table 4): tight binding of mutant enzymes to uracil-containing DNA and weak binding of wild-type and mutant enzymes to product DNA and both substrate analogs Ψrd and α-FdUrd.

Energetic Analysis of DNA Binding—The equilibrium dissociation constants determined above can be considered in energetic terms because the dissociation constant provides a measure of the Gibbs free energy for the binding reaction according to Equation 2,

$$\Delta G = -RT \ln(1/K_d) \quad \text{(Eq. 2)}$$

where R is the gas constant (1.987 cal degree^{-1} mol^{-1}).

The binding of human D145N/H268N UNG to the single-stranded HU oligonucleotide has a free energy of −10.6 kcal mol^{-1}. The equivalent abasic oligonucleotide has a ΔG of −7.4 kcal mol^{-1}. The absence of the uracil base thus leads to a $\Delta\Delta G$ of −3.2 kcal mol^{-1}, which is a significant proportion of the binding energy. A more modest loss in binding energy of −1.2 kcal mol^{-1} was observed upon going from single- to double-stranded DNA (HU *versus* HU·G), which is most likely due to the distortions that the enzyme must exert on the DNA. However, with the abasic DNAs, there was no loss of binding energy between single- and double-stranded forms (HAP *versus* HAP·G), suggesting that the DNA is less distorted in the enzyme-product complex. These values are remarkably consistent across both the human and HSV-1 UNG enzymes.

Further analysis of binding energies between the wild-type and single and double mutant forms of the human and HSV-1 UNG enzymes with Ψrd and α-FdUrd analogs did not reveal any significant coupling of binding energy between these two mutations: for hUNG with Ψrd, the coupling energy ($\Delta\Delta G$) between the D145N and H268N mutations is +0.62 kcal mol^{-1}. The absence of any negative coupling energy implies that these catalytic residues do not cooperate in straining the substrate prior to catalysis. Alternatively, UNG may not be able to fully flip these base analogs into the active site, so they may not be able to interact with the catalytic residues.

Structural Comparison of the HSV-1 Wild-type and D88N/H210N UNG Enzymes—The DNA binding data presented above indicate that the mutant enzymes bind uracil-containing DNA tightly, whereas abasic product DNA is bound weakly. To further explore the mechanism of base recognition by mutant UNG compared with wild-type UNG, we used x-ray crystallography to investigate these interactions at the atomic level.

The crystal structure of free HSV-1 D88N/H210N UNG was refined to 2.1-Å resolution. The structure lacks electron density for the first 16 amino acid residues, and these residues are presumed to be disordered in the crystal. This phenomenon is also observed in the HSV-1 wild-type UNG crystal (5). Superimposition of the mutant structure with that of HSV-1 wild-type UNG indicates that the double mutation of Asp^{88} and His^{210} to Asn caused no major changes in either the overall structure or the positions of critical amino acid residues involved in the formation of the uracil-binding pocket (Fig. 6*A*).

Electron density maps reveal that the His residue in the active site (His^{210}) was successfully mutated to asparagine and adopted the same conformation. Amino acid 88 in D88N/H210N UNG adopted a different orientation in comparison with Asp^{88} in the wild-type enzyme (Fig. 6*A*). The Asn^{88} side chain in D88N/H210N UNG is turned away from the active site, whereas the Asp^{88} side chain in wild-type UNG is pointed toward the active site. The position of the Asn^{88} side chain in the D88N/H210N UNG crystal is similar to the Asp^{88} side chain in the trinucleotide complex crystal (5), where Asp^{88} is rotated away from deoxythymidine, and this orientation is presumed to be involved in the rejection of thymidine as a substrate (5). Consistent with this, the position of the side chain of Asn^{88} is most likely a factor causing a decrease in the activity of D88N UNG.

The crystal structure of HSV-1 D88N/H210N UNG soaked with uridine has been solved to 1.8-Å resolution. Electron density maps show that there is electron density corresponding to the *N*-glycosidic bond, consistent with the lack of catalytic activity observed with this mutant in biochemical assays (Fig. 3). Some disordered density is observed in the region of the deoxyribose. The disordering is most likely due to rotation around the *N*-glycosidic bond and possibly also to fragmentation of the labile deoxyribose by high intensity ionizing radiation during data collection.

The D88N/H210N UNG-uracil complex structure reveals that the uracil is bound in exactly the same position as in the binding pocket of the wild-type enzyme (Fig. 6*B*). The uracil contributes a number of hydrogen bonds with amino acid residues in the binding pocket (Fig. 6*C*). These interactions in HSV-1 D88N/H210N UNG are similar to those in the wild-type enzyme (Fig. 6*C*). The rotation of Asn^{88} away from the position of Asp^{88} in the wild-type structure does not affect the binding of the uracil, nor does the mutation of His^{210} to Asn. These results clearly demonstrate that HSV-1 D88N/H210N UNG binds uracil in the same manner as the wild-type enzyme.

We also attempted to solve the structure of the Ψrd nucleotide in complex with UNG with the objective of investigating the atomic interactions of this analog with the active site of the enzyme. The structure of hUNG has been previously solved in complex with an oligonucleotide containing Ψrd, and a distorted conformation of the *N*-glycosidic bond was observed (35). Here, we were concerned primarily with interactions

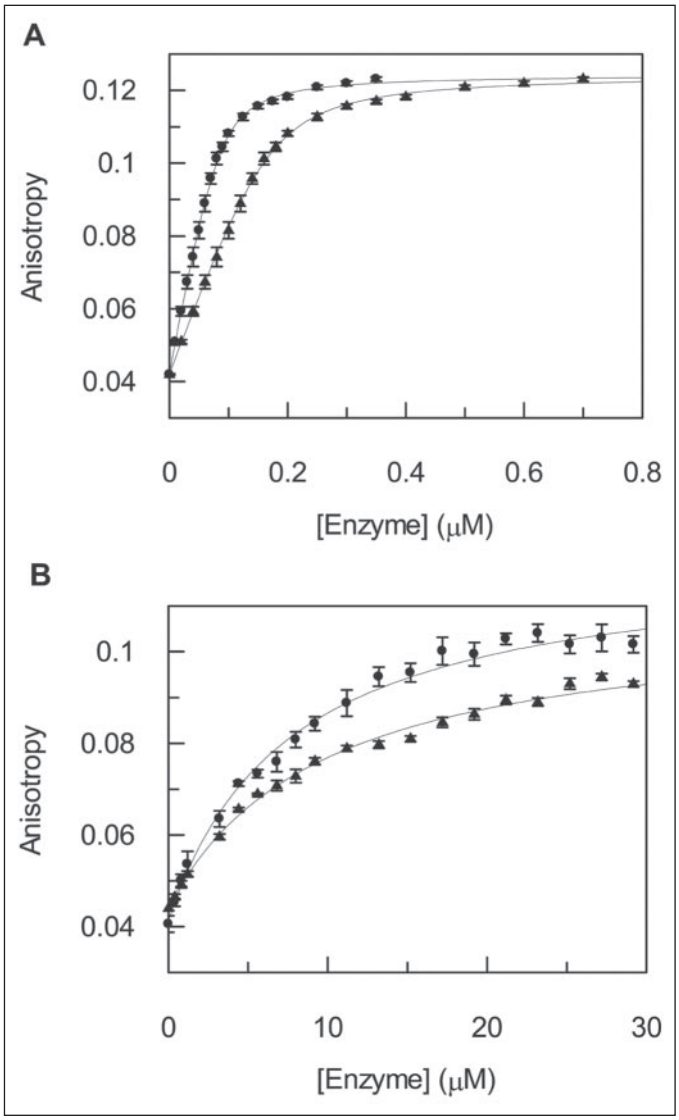

FIGURE 4. **Binding of wild-type and mutant hUNG enzymes to native DNAs.** *A*, equilibrium DNA binding experiments were performed with human D145N/H268N UNG and the HU and HU·G oligonucleotides by fluorescence anisotropy (see "Materials and Methods"). The increase in anisotropy for the binding of hUNG to the HU (●) and HU·G (▲) oligonucleotides is shown plotted against enzyme concentration. Data are shown with the best fit to the binding equation with the following values: HU, $K_d = (0.016 \pm 2) \times 10^{-3}$ μM, $A_D = 0.042 \pm 0.001$, and $A_{DE} = 0.12 \pm 0.001$; and HU·G, $K_d = (0.130 \pm 8) \times 10^{-3}$ μM, $A_D = 0.061 \pm 0.001$, and $A_{DE} = 0.12 \pm 0.001$. *B*, the binding of wild-type hUNG to HAP (●) and HAP·G (▲) abasic DNAs was determined by fluorescence anisotropy and is shown plotted against enzyme concentration. Data are shown with the best fit to the binding equation with the following values: HAP, $K_d = 6.9 \pm 0.7$ μM, $A_D = 0.042 \pm 0.001$, and $A_{DE} = 0.12 \pm 0.002$; and HAP·G, $K_d = 9.0 \pm 0.8$ μM, $A_D = 0.041 \pm 0.001$, and $A_{DE} = 0.12 \pm 0.001$.

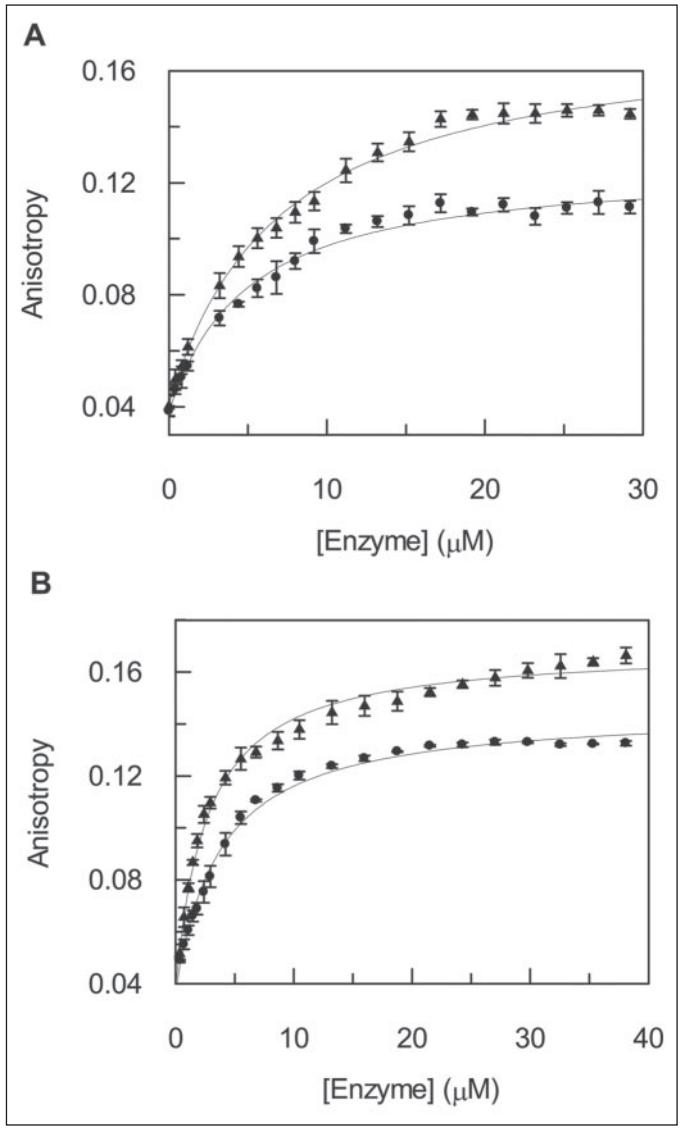

FIGURE 5. **Binding of the human wild-type and D145N/H268N UNG enzymes to non-cleavable substrate analogs dΨrd and α-FdUrd.** The binding of hexachlorofluorescein-labeled oligonucleotides containing the non-cleavable substrate analogs dΨrd and α-FdUrd was monitored using fluorescence polarization. *A*, the binding of wild-type hUNG was measured with dΨrd (●) and α-FdUrd (▲). Data are shown with the best fit to the binding equation with the following values: dΨrd, $K_d = 4.4 \pm 0.5$ μM, $A_D = 0.041 \pm 0.002$, and $A_{DE} = 0.17 \pm 0.003$; and α-FdUrd, $K_d = 6.3 \pm 0.6$ μM, $A_D = 0.039 \pm 0.002$, and $A_{DE} = 0.13 \pm 0.002$. *B*, the binding of human D145N/H268N UNG was measured with dΨrd (●) and α-FdUrd (▲). Data are shown with the best fit to the binding equation with the following values: dΨrd, $K_d = 3.2 \pm 0.2$ μM, $A_D = 0.038 \pm 0.001$, and $A_{DE} = 0.14 \pm 0.001$; and α-FdUrd, $K_d = 2.2 \pm 0.2$ μM, $A_D = 0.041 \pm 0.003$, and $A_{DE} = 0.17 \pm 0.002$.

of the base with the active-site pocket of the mutant enzyme and whether the free nucleotide would adopt the same distorted conformation in the D88N/H210N mutant enzyme. However, despite efforts to both soak and co-crystallize the mutant enzyme with Ψrd under a wide range of conditions, we were unable to obtain a complex. We consider that the weak binding of the Ψrd oligonucleotide reflects a poor interaction of the enzyme with the pseudouracil base and that, for this reason, we were unable to obtain a complex of HSV-1 D88N/H210N UNG with Ψrd.

DISCUSSION

Implications of the Catalytic Activity of UNG—In this study, the human and HSV-1 UNG enzymes were compared using a combination of steady-state kinetics and equilibrium binding. The steady-state assays showed that there is a significant difference in the specificity constant (k_{cat}/K_m) for these two UNG forms (Table 3). Examination of the kinetic constants showed that the human enzyme has a much lower K_m compared with the viral enzyme, resulting in its having a higher specificity constant.

The K_m values that we obtained for hUNG with uracil in single-stranded DNA (0.22 μM), the U·G mismatch (0.1 μM), and the U·A base pair (0.12 μM) are significantly lower than the previous measurements of 0.4 and 4.5 μM for single-stranded and U·A substrates, respectively (12). These other measures of catalytic constants for hUNG were obtained upon the release of [^{3}H]uracil in U·A base pairs from calf thymus DNA (8, 12, 13). The somewhat higher k_{cat} values obtained from this assay (~20 s^{-1}) may reflect the processivity of the enzyme releasing

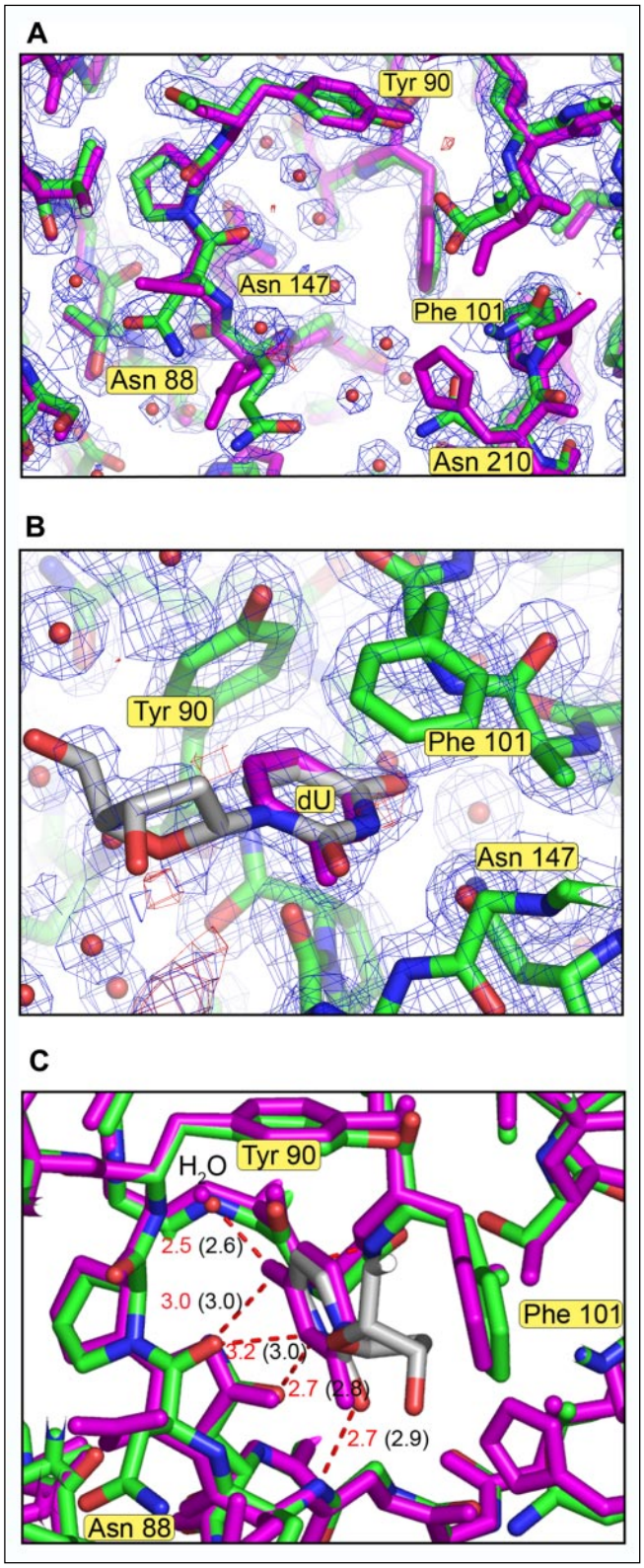

FIGURE 6. **Active site of HSV-1 D88N/H210N UNG.** *A*, the amino acid residues in the active site of HSV-1 D88N/H210N UNG (*green*, carbons; *blue*, nitrogen; *red*, oxygens) are aligned with those of the wild-type enzyme (*purple*). Electron density for HSV-1 D88N/H210N UNG is shown. *B*, HSV-1 D88N/H210N UNG with uridine bound in the active site is aligned with the wild-type enzyme with uracil bound in the active site (*purple*). Electron density for HSV-1 D88N/H210N UNG is shown. *C*, hydrogen bond distances between the residues in the HSV-1 D88N/H210N UNG active site and the bound uracil are shown in *red*, whereas those in the active site of the wild-type enzyme are shown in *black*.

many uracil bases from the same DNA molecule. The K_m values obtained from this assay range from 0.1 to 4.5 μM, but vary according to the conditions used and cannot be related to specific sequences due to the nature of the assay. These high K_m values have led to the proposition that hUNG acts solely in the post-replicative repair of U·A mismatches (14).

Our previous study with HSV-1 UNG demonstrated that sequence context can be an important factor in enzyme activity and that variations in K_m of an order of magnitude may be expected, although k_{cat} is quite insensitive (10). In this study, we used the same AT-rich substrate that we employed previously, which gave lower K_m values (10). Furthermore, hUNG exhibits no marked preference between U·G mismatches and U·A mispairs (Table 3). This is in agreement with previously published data suggesting that UNG is more sensitive to the sequence context of uracil than to the partner base of uracil (10).

In principle, k_{cat}/K_m provides a measure of the relative efficiency with which an enzyme discriminates between two substrates present in the same reaction mixture (36). The k_{cat}/K_m value for hUNG with U·G mismatches (74 μM^{-1} s^{-1}) is significantly higher than the value for *Xenopus* SMUG1 with U·G mismatches (0.04 μM^{-1} s^{-1}) (37). However, *Xenopus* SMUG1 has been shown to be rate-limited by its product dissociation from double-stranded DNA, but *Xenopus* SMUG1 is stimulated by AP endonuclease, the subsequent enzyme in the base excision repair pathway (13, 14). The specificity constant may thus not provide an accurate picture of substrate discrimination *in vivo*.

A comparison of our K_m value for hUNG with U·G mismatches (0.1 μM) with the K_m value for *Xenopus* SMUG1 with U·G mismatches (0.035 μM) shows that there is not a significant difference. Although *Xenopus* SMUG1 is evidently capable of removing uracil from U·G mismatches from substrates at low concentration (14), our data demonstrate that there will not be stringent discrimination between U·A and U·G substrates by hUNG and *Xenopus* SMUG1 based on their kinetic parameters.

A recent study demonstrated that *Ung*$^{-/-}$/SMUG ↓ mouse embryonic fibroblast cells are more sensitive to γ-radiation compared with cell lines that carry just the individual mutations (38). This clearly indicates degeneracy in the activity of these two enzymes against a lethal lesion. The same study also showed that C-to-T mutation frequency is largely, although not completely, additive. The C-to-T mutation frequency in *Ung*$^{-/-}$ cells relative to SMUG ↓ cells indicates that UNG is involved in the repair of U·G mismatches *in vivo*, which might be due to an increase in deamination during DNA replication. The largely additive response suggests some specialization for the two enzymes, possibly through compartmentalization and control (38).

There is evidence for the control of hUNG from its localization at replication foci (39) and controlled degradation during S phase (40). However, the high catalytic turnover of hUNG means that, even at barely detectable levels, it may still be a significant anti-mutator, and there is evidently no survival disadvantage from degeneracy in DNA repair systems. The observed control may thus reflect the requirement to significantly up-regulate repair during DNA replication. Although it is clear that hUNG has a role in the post-replicative repair of uracil (39–41), our data support the hypothesis that hUNG will operate on both U·A and U·G lesions *in vivo* and will thus have some overlapping activity with SMUG1 against U·G mismatches and other lesions.

Base Excision by UNG Is Uncoupled from Abasic Site Recognition—DNA binding assays demonstrated that the catalytically inactive human D145N/H268N and HSV-1 D88N/H210N UNG double mutants were able to bind uracil-containing DNA tightly (Table 4). The crystal structure of HSV-1 D88N/H210N UNG in complex with uracil shows that

the base is bound in the active site of the enzyme in exactly the same way as it is bound in the wild-type enzyme (Fig. 6, *B* and *C*). The specific interactions between the base and the active-site amino acids remain unaltered. We therefore conclude that the active-site mutations do not interfere with substrate binding, but solely with the catalytic mechanism.

In contrast to the tight binding to the uracil-containing DNA, both the human and HSV-1 wild-type and mutant UNG enzymes exhibited ~100-fold weaker binding to the abasic product DNA (Table 4). These results contradict those previously obtained with hUNG predicting abasic site protection and coupling to the subsequent base excision repair machinery (9). This previous study used surface plasmon resonance to measure DNA binding, whereas we employed a solution-based technique that is free of many of the deviations that can arise with surface plasmon resonance. Furthermore, our results (Table 4) are completely consistent with our previous data obtained with UNG from HSV-1 (10) as well as with the observed lack of AP site inhibition with hUNG (13, 42).

The crystal structures of UNG in complex with uracil show that the amino acids in the active site of UNG can form a number of interactions with the bound uracil (Fig. 6*C*). These interactions are likely to be responsible for the tight binding of UNG to the uracil-containing DNA. Consistent with this, the lack of these specific interactions in abasic product DNA gives rise to the low affinity of UNG for AP sites described above.

UNG activity has been shown to increase upon addition of human AP endonuclease (HAP-1), suggesting that HAP-1 promotes AP site release by UNG and couples the steps of base excision repair (9). However, the enhancement of UNG activity increases with increasing concentrations of AP endonuclease up to 50-molar excess, whereas a stoichiometric amount of HAP-1 does not increase activity. Furthermore, the difference in activity is more apparent at later reaction time points. Because UNG is weakly inhibited by abasic DNA *in vitro* (13, 42), the previously observed enhancement of UNG activity by HAP-1 is consistent with the removal of accumulating AP sites. Our data clearly show that UNG has a low affinity for abasic sites and that the enzyme has a high turnover rate, which is inconsistent with AP site protection by UNG. Although there is a clear appeal to having a coupling of DNA glycosylase and AP endonuclease activities, we can find no data that support such a theory for either human or HSV-1 UNG.

DNA Binding and Base Recognition by UNG—Previous crystallographic studies with hUNG clearly showed the enzyme flipping its target nucleotide out of the DNA double helix and into the enzyme active site (8). Our binding data with both human and HSV-1 UNG mutants demonstrate that it gains a large part of its binding energy from interactions with the uracil base. Furthermore, our crystallographic studies demonstrated that the double mutant enzyme binds the uracil base in exactly the same way as the wild-type enzyme. We therefore conclude that the active-site His and Asp residues do not contribute to uracil binding, but have a solely catalytic role. The double mutant enzymes thus provide a sound basis for investigating protein-DNA interactions of UNG enzymes.

An unexpected finding of this study was the weak binding of both non-cleavable substrate analogs that we tested: dΨrd and α-FdUrd. The dΨrd analog has been previously used to obtain the structure of an enzyme-substrate complex (35). In this structure, hUNG is bound to DNA, with the dΨrd flipped out of the DNA double helix into the active site. The ring of dΨrd is rotated 90° on the glycosidic bond, and C-1 adopts a tetrahedral conformation. This is a highly unusual nucleotide conformation and led to the proposition that UNG exerts a physical strain on the substrate, which leads to enhanced electron orbital overlap, thus facilitating catalysis (35).

An alternative explanation for the conformation of dΨrd observed in the complex with UNG is that a tautomerization has taken place, which leads to sp^3-hybridized C-1. It is noteworthy that N-5 of dΨrd becomes significantly more acidic than N-1 in uracil (43), and this may provide a mechanism for protonation of C-1. This is an energetically unfavorable process because it would lead to the loss of aromaticity. However, the crystals with the dΨrd oligonucleotides took 2 months to grow compared with 1 week for crystals with native DNA (6, 8). It is thus possible either that this unfavorable tautomer is slowly produced and then captured by UNG or that the tautomerization is relatively facile and is the reason for the poor binding that we observed. Our results demonstrate that caution needs to be used when interpreting experiments with both dΨrd and α-FdUrd because UNG clearly does not behave in the same way with these base analogs as it does with native uridine.

Conclusion—We have performed a kinetic analysis of both human and HSV-1 UNG enzymes using oligonucleotide substrates to monitor both DNA binding and catalytic activity. The striking feature of this analysis is the similarity of the two enzymes. hUNG has a notably higher k_{cat}/K_m, suggesting that it is evolutionarily better adapted to removing minor bases from a large genome. In all other respects, these two enzymes possess a remarkable similarity in function given their 39% sequence identity. Considering also the great similarity of their structures, it seems that the viral enzyme would be a difficult target for specific therapeutics.

The kinetic parameters that we determined for hUNG also have significant implications for the proposed function of this enzyme. We have demonstrated that hUNG has a low K_m and a high k_{cat}/K_m for both U·A and U·G substrates. We therefore conclude that it is unlikely to be a specific U·A glycosylase *in vivo*, but that it will most likely have overlapping U·G activity with the SMUG1 DNA glycosylase. Furthermore, the high K_d that we observed for hUNG with abasic DNA suggests that its activity will be uncoupled from the subsequent common steps of base excision repair initiated by the AP endonuclease.

Acknowledgments—We thank Dr. Bernard O'Hara for assistance in x-ray data collection and the Daresbury Synchrotron Radiation Source for access to synchrotron beam time.

REFERENCES

1. Lindahl, T. (1993) *Nature* **362,** 709–715
2. Lindahl, T. (1974) *Proc. Natl. Acad. Sci. U. S. A.* **71,** 3649–3653
3. Seeberg, E., Eide, L., and Bjoras, M. (1995) *Trends Biochem. Sci.* **20,** 391–397
4. Barzilay, G., and Hickson, I. D. (1995) *BioEssays* **17,** 713–719
5. Savva, R., McAuley-Hecht, K., Brown, T., and Pearl, L. (1995) *Nature* **373,** 487–493
6. Mol, C. D., Arvai, A. S., Slupphaug, G., Kavli, B., Alseth, I., Krokan, H. E., and Tainer, J. A. (1995) *Cell* **80,** 869–878
7. Xiao, G. Y., Tordova, M., Jagadeesh, J., Drohat, A. C., Stivers, J. T., and Gilliland, G. L. (1999) *Proteins* **35,** 13–24
8. Slupphaug, G., Mol, C. D., Kavli, B., Arvai, A. S., Krokan, H. E., and Tainer, J. A. (1996) *Nature* **384,** 87–92
9. Parikh, S. S., Mol, C. D., Slupphaug, G., Bharati, S., Krokan, H. E., and Tainer, J. A. (1998) *EMBO J.* **17,** 5214–5226
10. Bellamy, S. R., and Baldwin, G. S. (2001) *Nucleic Acids Res.* **29,** 3857–3863
11. Panayotou, G., Brown, T., Barlow, T., Pearl, L. H., and Savva, R. (1998) *J. Biol. Chem.* **273,** 45–50
12. Slupphaug, G., Eftedal, I., Kavli, B., Bharati, S., Helle, N. M., Haug, T., Levine, D. W., and Krokan, H. E. (1995) *Biochemistry* **34,** 128–138
13. Kavli, B., Sundheim, O., Akbari, M., Otterlei, M., Nilsen, H., Skorpen, F., Aas, P. A., Hagen, L., Krokan, H. E., and Slupphaug, G. (2002) *J. Biol. Chem.* **277,** 39926–39936
14. Nilsen, H., Haushalter, K. A., Robins, P., Barnes, D. E., Verdine, G. L., and Lindahl, T. (2001) *EMBO J.* **20,** 4278–4286
15. Sekino, Y., Bruner, S. D., and Verdine, G. L. (2000) *J. Biol. Chem.* **275,** 36506–36508
16. Sambrook, J., Fritsch, E. F., and Maniatis, T. (1989) *Molecular Cloning: A Laboratory*

Manual, Cold Spring Harbor Laboratory, Cold Spring Harbor, NY
17. Baldwin, G. S., Vipond, I. B., and Halford, S. E. (1995) *Biochemistry* **34,** 705–714
18. O'Neill, R. J., Vorob'eva, O. V., Shahbakhti, H., Zmuda, E., Bhagwat, A. S., and Baldwin, G. S. (2003) *J. Biol. Chem.* **278,** 20526–20532
19. Reid, S. L., Parry, D., Liu, H. H., and Connolly, B. A. (2001) *Biochemistry* **40,** 2484–2494
20. Vagin, A., and Teplyakov, A. (1997) *J. Appl. Crystallogr.* **30,** 1022–1025
21. Brunger, A. T., Adams, P. D., Clore, G. M., DeLano, W. L., Gros, P., Grosse-Kunstleve, R. W., Jiang, J., Kuszewski, J., Nilges, M., Pannu, N. S., Read, R. J., Rice, L. M., Simonson, T., and Warren, G. L. (1998) *Acta Crystallogr. Sect. D* **54,** 905–921
22. Jones, T. A., Zou, J. Y., and Cowan, S. W. (1991) *Acta Crystallogr. Sect. A* **47,** 110–119
23. Perrakis, A. P., Sixma, T. K., Wilson, K. S., and Lamzin, V. S. (1997) *Acta Crystallogr. Sect. D* **53,** 448–455
24. Laskowski, R. A., MacArthur, M. W., Moss, D. S., and Thornton, J. M. (1993) *J. Appl. Crystallogr.* **26,** 283–291
25. Vriend, G. (1990) *J. Mol. Graphics* **8,** 52–56
26. Law, S. M., Eritja, R., Goodman, M. F., and Breslauer, K. J. (1996) *Biochemistry* **35,** 12329–12337
27. Stivers, J. T. (1998) *Nucleic Acids Res.* **26,** 3837–3844
28. Drohat, A. C., Jagadeesh, J., Ferguson, E., and Stivers, J. T. (1999) *Biochemistry* **38,** 11866–11875
29. Uesugi, S., Miki, H., Ikehara, M., Iwahashi, H., and Kyogoku, Y. (1979) *Tetrahedron Lett.* **20,** 4073–4076
30. Williams, D. M., Benseler, F., and Eckstein, F. (1991) *Biochemistry* **30,** 4001–4009
31. Fazakerley, G. V., Uesugi, S., Izumi, A., Ikehara, M., and Guschlbauer, W. (1985) *FEBS Lett.* **182,** 365–369
32. Marck, C., Lesyng, B., and Saenger, W. (1982) *J. Mol. Struct.* **82,** 77–94
33. Stivers, J. T., Pankiewicz, K. W., and Watanabe, K. A. (1999) *Biochemistry* **38,** 952–963
34. Powell, L. M., Connolly, B. A., and Dryden, D. T. (1998) *J. Mol. Biol.* **283,** 947–961
35. Parikh, S. S., Walcher, G., Jones, G. D., Slupphaug, G., Krokan, H. E., Blackburn, G. M., and Tainer, J. A. (2000) *Proc. Natl. Acad. Sci. U. S. A.* **97,** 5083–5088
36. Cornish-Bowden, A. (2001) *Fundamentals of Enzyme Kinetics*, Portland Press Ltd., London
37. Haushalter, K. A., Stukenberg, P. T., Kirschner, M. W., and Verdine, G. L. (1999) *Curr. Biol.* **9,** 174–185
38. An, Q., Robins, P., Lindahl, T., and Barnes, D. E. (2005) *EMBO J.* **24,** 2205–2213
39. Otterlei, M., Warbrick, E., Nagelhus, T. A., Haug, T., Slupphaug, G., Akbari, M., Aas, P. A., Steinsbekk, K., Bakke, O., and Krokan, H. E. (1999) *EMBO J.* **18,** 3834–3844
40. Fischer, J. A., Muller-Weeks, S., and Caradonna, S. (2004) *DNA Repair* **3,** 505–513
41. Nilsen, H., Rosewell, I., Robins, P., Skjelbred, C. F., Andersen, S., Slupphaug, G., Daly, G., Krokan, H. E., Lindahl, T., and Barnes, D. E. (2000) *Mol. Cell* **5,** 1059–1065
42. Jiang, Y. L., Ichikawa, Y., and Stivers, J. T. (2002) *Biochemistry* **41,** 7116–7124
43. Lipnick, R. L., Fissekis, J. D., and O'Brien, J. P. (1981) *Biochemistry* **20,** 7319–7327

A Comparative Study of Uracil-DNA Glycosylases from Human and Herpes Simplex Virus Type 1

Kuakarun Krusong, Elisabeth P. Carpenter, Stuart R. W. Bellamy, Renos Savva and Geoff S. Baldwin

J. Biol. Chem. 2006, 281:4983-4992.
doi: 10.1074/jbc.M509137200 originally published online November 22, 2005
